

Trapped unitary two-component Fermi gases with up to ten particles

X. Y. Yin¹ and D. Blume¹

¹*Department of Physics and Astronomy, Washington State University, Pullman, Washington 99164-2814, USA*

(Dated: September 15, 2021)

The properties of two-component Fermi gases with zero-range interactions are universal. We use an explicitly correlated Gaussian basis set expansion approach to investigate small equal-mass two-component Fermi gases under spherically symmetric external harmonic confinement. At unitarity, we determine the ground state energy for systems with up to ten particles interacting through finite-range two-body potentials for both even and odd number of particles. We extrapolate the energies to the zero-range limit using a novel scheme that removes the linear and, in some cases, also the quadratic dependence of the ground state energies on the two-body range. Our extrapolated zero-range energies are compared with results from the literature. We also calculate the two-body Tan contact and structural properties.

PACS numbers: 03.75.Ss, 34.50.Cx

I. INTRODUCTION

The properties of two-component Fermi gases interacting through two-body zero-range potentials with s -wave scattering length a_s are universal [1, 2]. At unitarity, i.e., for infinitely large a_s , the two-body interaction does not define a meaningful length scale and the strongly-interacting Fermi gas is characterized by the same number of length scales as the non-interacting Fermi gas. Approximate realizations of the unitary Fermi gas include dilute neutron matter in the crusts of neutron stars [3] and ultracold atom gases such as ⁶Li [4] and ⁴⁰K [5]. The properties of homogeneous and inhomogeneous unitary Fermi gases have attracted a great deal of experimental and theoretical attention. For spherically symmetric external confinement, the harmonic oscillator length a_{ho} defines the only length scale of the system. It is hence interesting to determine how the properties of trapped unitary Fermi gases vary with the number of particles.

Harmonically trapped Fermi gases at unitarity have been treated by quantum Monte Carlo methods [6–13], density functional theory (DFT) [11, 14–17], and basis set expansion approaches. The accuracy of the fixed-node diffusion Monte Carlo (FN-DMC) energies [7, 8, 11, 12] depends on the quality of the many-body nodal surface. The resulting energies provide upper bounds to the exact ground state energies and the zero-range limit is reached through extrapolation [11, 12]. Auxiliary-field quantum Monte Carlo (AFMC) methods, on the other hand, work on a finite lattice and extrapolation to the infinite lattice limit is required to obtain fully converged result [12]. The quality of DFT calculations depends critically on the underlying functional. Since the functional is typically obtained by matching to data for the homogeneous system, the analysis of results for the trapped system can provide insights into gradient corrections and other finite size features [15–17]. Trapped unitary Fermi gases with up to six particles have been calculated by explicitly correlated Gaussian (ECG) basis set expansion approaches [7, 8, 18–22] with better than about 1% accuracy. Application of the ECG method to systems with more than six particles

has been challenging due to the rapid increase of the number of permutations and the larger number of degrees of freedom. Recently, Ref. [23] treated the $(N_1, N_2) = (4, 4)$ system at unitarity using a basis set that accounts for the most important but not all correlations.

Here, we present results for small trapped unitary Fermi gases with $N \leq 10$ particles, where $N = N_1 + N_2$ and $N_1 - N_2 = 0$ or 1. Our extrapolated zero-range energy of the (4,4) system is 0.9% lower than that reported in Ref. [23]. A new aspect of our work is that we developed an improved scheme for extrapolating the finite-range energies to the zero-range limit. This new scheme eliminates the linear and, in some cases, the quadratic dependence of the ground state energies on the two-body range. The scheme provides a consistency check on the range-dependence of our energies and reduces the errors that result from the extrapolation to the zero-range limit. Our results suggest that the developed range correction scheme allows one to obtain a reliable approximation to the zero-range energy from a single finite-range calculation. The scheme can be applied to other numerical calculations that work with finite-range interactions. We use our range correction scheme to determine the zero-range energies and the Tan contact for two-component Fermi gases with $N \leq 10$ at unitarity. In addition, we present selected structural properties.

The remainder of this paper is organized as follows. Section II discusses the theoretical framework and our extrapolation scheme to the zero-range limit. Section III presents our results for systems with up to ten particles and compares, where available, with results from the literature. Lastly, Sec. IV concludes.

II. THEORETICAL FRAMEWORK

We consider equal-mass two-component Fermi gases with N_1 spin-up and N_2 spin-down atoms ($N = N_1 + N_2$ and $N_1 - N_2 = 0$ or 1) under external spherically symmetric harmonic confinement with angular trapping

frequency ω . The system Hamiltonian $H(r_0)$ reads

$$H(r_0) = \sum_{i=1}^N -\frac{\hbar^2}{2m} \nabla_i^2 + V_{\text{tr}}(\vec{r}_1, \dots, \vec{r}_N) + \sum_{i=1}^{N_1} \sum_{j=N_1+1}^N V_{2b}(r_{ij}, r_0), \quad (1)$$

where m denotes the atom mass, \vec{r}_i denotes the position vector of the i th particle with respect to the trap center, and

$$V_{\text{tr}}(\vec{r}_1, \dots, \vec{r}_N) = \sum_{i=1}^N \frac{1}{2} m \omega^2 \vec{r}_i^2 \quad (2)$$

is the trapping potential. V_{2b} is the interspecies two-body interaction potential that depends on the interparticle distance r_{ij} , $r_{ij} = |\vec{r}_i - \vec{r}_j|$. In our work, it is modeled by a finite-range Gaussian potential with range r_0 and depth V_0 ($V_0 < 0$),

$$V_{2b}(r, r_0) = V_0 \exp\left(-\frac{r^2}{2r_0^2}\right). \quad (3)$$

For a fixed r_0 , V_0 is adjusted such that $V_{2b}(r, r_0)$ has an infinitely large s -wave scattering length a_s and supports one zero-energy two-body bound state in free space. The ranges r_0 considered depend on the size of the system and vary from $0.01a_{\text{ho}}$ to $0.12a_{\text{ho}}$, where a_{ho} denotes the harmonic oscillator length [$a_{\text{ho}} = \sqrt{\hbar/(m\omega)}$]. For the Gaussian potential with one zero-energy bound state, the effective range r_{eff} is approximately equal to $2.032r_0$.

To numerically solve the Schrödinger equation for the Hamiltonian given in Eq. (1), we separate off the center of mass degrees of freedom and expand the eigenstates of the relative Hamiltonian in terms of ECG basis functions, which depend on a set of non-linear variational parameters that are optimized through energy minimization (see below) [18, 24]. The unsymmetrized basis functions for states with $L^\pi = 0^+$ and 1^- symmetry (L denotes the relative orbital angular momentum and π the relative parity) read $\exp(-\frac{1}{2}\vec{x}^T A \vec{x})$ and $\mathcal{Y}_{10}(\vec{u}^T \vec{x}) \exp(-\frac{1}{2}\vec{x}^T A \vec{x})$, respectively, where A is a symmetric and positive definite $(N-1) \times (N-1)$ parameter matrix, $\vec{u} = (u_1, u_2, \dots, u_{N-1})^T$ is a $N-1$ dimensional vector, and \mathcal{Y}_{10} is a solid spherical harmonic function [24]. $\vec{x} = (\vec{x}_1, \vec{x}_2, \dots, \vec{x}_{N-1})^T$ collectively denotes a set of $N-1$ Jacobi vectors. The ground state of even N systems has 0^+ symmetry and that of odd N systems has 1^- symmetry. A key advantage of these basis functions is that the corresponding overlap and Hamiltonian matrix elements can be calculated analytically [24].

The fermionic exchange symmetry is ensured by acting with the permutation operator \mathcal{A} on the unsymmetrized basis functions. The number of permutations N_p increases factorially with the number of identical fermions. For the $(5, 5)$ system, e.g., \mathcal{A} contains $(5!)^2 = 14,400$ two-particle exchange operations with alternating plus and

minus signs. The evaluation of each overlap and Hamiltonian matrix element involves a sum over N_p terms that are highly oscillatory. In a standard 16 digit floating point implementation, numerical challenges arise from the near-cancellation of the positive and negative terms for systems with $N > 8$. The near-cancellation of these terms of alternating signs can be interpreted as a relative of the fermion sign problem known from Monte Carlo simulations [25, 26]. To ensure that the matrix elements for the largest systems considered are accurate to at least ten significant digits, we implemented our C codes using extended precision. The eigenenergies and expansion coefficients are obtained by solving a generalized eigenvalue problem that involves the Hamiltonian matrix and the overlap matrix. The numerical error of the resulting eigenenergies is several orders of magnitude smaller than the errors that arise from the use of a finite basis set and the extrapolation to the zero-range limit. In Sec. III, we report the total ground state energy $E(r_0)$ of the Hamiltonian $H(r_0)$, i.e., we add the center of mass energy of $3E_{\text{ho}}/2$ to the relative energy obtained by the ECG approach. Here, E_{ho} denotes the harmonic oscillator energy ($E_{\text{ho}} = \hbar\omega$).

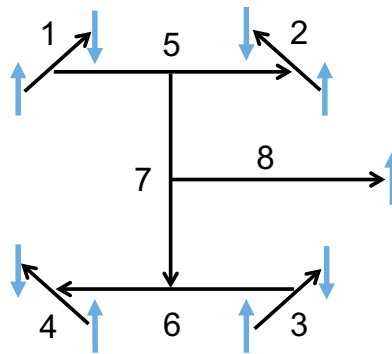


FIG. 1. (Color online) Illustration of the Jacobi coordinates employed in our work for the $(N_1, N_2) = (5, 4)$ system. The dark vectors show the Jacobi vectors $\vec{x}_1, \vec{x}_2, \dots, \vec{x}_8$. The spin-up and spin-down fermions are represented by light vertical up and down arrows.

We use a semi-stochastic variational approach to choose and optimize the variational parameters contained in A and \vec{u} [24]. Our Jacobi coordinates are chosen such that the first N_2 Jacobi vectors correspond to distance vectors between unlike particle pairs. The next $N_2/2$ Jacobi vectors correspond to the distance vectors between the center of mass of the first pair and the second pair, the distance vector between the center of mass of the third pair and the fourth pair, and so on. The remaining Jacobi vectors connect the larger sub-units and, for odd N , the N th particle (see Fig. 1 for an illustration for $N = 9$). For this choice of Jacobi coordinates, the first N_2 diagonal elements of the A matrix represent correlations between unlike particles. We expect that these interspecies distances are, on average, smaller and more strongly correlated than those between like particles. This motivates

us to choose the first N_2 diagonal elements of the A matrix for each basis function from a preset non-linear grid. The other diagonal elements are chosen stochastically from preset parameter windows. As in Ref. [23], we start with basis functions that are diagonal in A . These basis functions account for the most important correlations. Once a certain basis set size is reached (for the larger systems around $N_b = 500$), we reoptimize the variational parameters contained in the diagonal of A , and for odd N in \vec{u} , and allow for off-diagonal A matrix elements. The off-diagonal matrix element at position (i, j) of the A matrix is chosen from 0 to the geometric mean of the i th and j th diagonal elements. We find that this choice results with high probability in positive-definite A matrices. The positive-definiteness of the A matrix is tested through diagonalization. We refer to the reoptimization of all variational parameters contained in A and, if applicable, \vec{u} of all N_b basis functions as a reoptimization cycle. The re-optimization cycle is repeated until the lowest energy changes by less than a preset value. After that, we extend the basis set by a hundred to several hundred basis functions and reoptimize the variational parameters of the enlarged basis set using a variable number of reoptimization cycles. This process is repeated a few times. At the end, the basis is enlarged to around 2000 basis functions without additional reoptimization of the non-linear variational parameters. The basis set errors reported in Tables I and II of Sec. III and Tables I-VI of the Supplemental Material [27] are estimated by analyzing the energy decrease that results from the basis set enlargements and the reoptimization cycles.

To reach the universal regime where a_{ho} defines the only length scale in the system, we need to extrapolate the numerically calculated finite-range energies to the zero-range limit. In previous ECG works [18, 19, 21–23], this was done by fitting the finite-range energies by a linear or quadratic function. We refer to this traditional extrapolation scheme as the zeroth-order extrapolation scheme. The difference between the finite-range energies and the extrapolated zero-range energies is, typically, at the order of a few percent and can introduce a non-negligible extrapolation error. Moreover, for larger systems, it is computationally expensive, maybe even prohibitively expensive, to obtain energies at very small ranges. It should also be noted that the extrapolated zero-range energies do not provide variational upper bounds even though the finite-range ECG energies do. It is thus desirable to remove the linear and, ideally, quadratic range dependence. Motivated by the generalized virial theorem

$$E(0) = 2V_{\text{tr}}(0) \quad (4)$$

[$V_{\text{tr}}(0)$ denotes the expectation value of $V_{\text{tr}}(\vec{r}_1, \dots, \vec{r}_N)$ for $r_0 \rightarrow 0$] at unitarity, Werner [28] proposed to remove the linear range-dependence of the ground state energy by combining it with the expectation value $V_{\text{tr}}(r_0)$ of the trapping potential $V_{\text{tr}}(\vec{r}_1, \dots, \vec{r}_N)$ calculated for the same

r_0 ,

$$E(0) = 3E(r_0) - 4V_{\text{tr}}(r_0) + \mathcal{O}(r_0^2). \quad (5)$$

While Eq. (5) removes the leading-order range dependence, it is associated with errorbars that come from the basis set errors of $E(r_0)$ and $V_{\text{tr}}(r_0)$. In our ECG method, the basis set is optimized by minimizing the ground state energy. Not surprisingly, we find that the convergence of the expectation value of the trapping potential is not as good as that of the energy. This motivates us to propose an alternative scheme that can be carried out to higher orders.

The ground state energy $E(r_0)$ of the N -particle system is a smooth function of the two-body interaction range r_0 . The n_{max} th order Taylor series of $E(\bar{r}_0)$ around r_0 is

$$E(\bar{r}_0) = \sum_{n=0}^{n_{\text{max}}} E^{(n)}(r_0) \frac{1}{n!} (\bar{r}_0 - r_0)^n + \mathcal{O}[(\bar{r}_0 - r_0)^{n_{\text{max}}+1}], \quad (6)$$

where

$$E^{(n)}(r_0) = \left. \frac{\partial^n E(\bar{r}_0)}{\partial \bar{r}_0^n} \right|_{\bar{r}_0=r_0} \quad (7)$$

is the n th order derivative of the ground state energy with respect to the range evaluated at r_0 . $E^{(0)}(r_0)$ is simply the ground state energy $E(r_0)$ of $H(r_0)$. $E^{(1)}(r_0)$ can be obtained through the Hellmann-Feynman theorem [29],

$$E^{(1)}(r_0) = \left\langle \left. \frac{\partial H(\bar{r}_0)}{\partial \bar{r}_0} \right|_{\bar{r}_0=r_0} \right\rangle, \quad (8)$$

which is exact in the limit that the basis set is complete. The matrix elements needed to evaluate $E^{(1)}(r_0)$ reduce to compact analytical expressions. $E^{(2)}(r_0)$ can be obtained by the finite difference method, i.e., by evaluating $E^{(1)}(r_0)$ at two nearby r_0 .

Our goal is to obtain the zero-range energy $E(0)$. Setting \bar{r}_0 in Eq. (6) to 0, we obtain

$$E(0) = E_{\text{ZRA}, n_{\text{max}}}(r_0) + \mathcal{O}(r_0^{n_{\text{max}}+1}), \quad (9)$$

where

$$E_{\text{ZRA}, n_{\text{max}}}(r_0) = \sum_{n=0}^{n_{\text{max}}} E^{(n)}(r_0) \frac{1}{n!} (-r_0)^n \quad (10)$$

is the n_{max} th order approximation to the zero-range energy. Equations (9) and (10) establish a relation between the zero-range energy $E(0)$ and the finite-range energy $E(r_0)$ and its derivatives with respect to the two-body range. $E_{\text{ZRA}, 0}(r_0)$ is simply the finite-range energy $E(r_0)$ with linear leading-order range-dependence. The leading-order range-dependence of $E_{\text{ZRA}, 1}(r_0)$ and $E_{\text{ZRA}, 2}(r_0)$ is quadratic and cubic, respectively. Crucial is that $E_{\text{ZRA}, 1}(r_0)$ and $E_{\text{ZRA}, 2}(r_0)$ are obtained at finite r_0 without extrapolation. They provide better approximations to the zero-range energy $E(0)$ than

$E_{\text{ZRA},0}(r_0)$. We refer to the extrapolations of $E_{\text{ZRA},1}(r_0)$ and $E_{\text{ZRA},2}(r_0)$ to the zero-range limit as the first- and second-order extrapolation schemes. For a complete basis, $E_{\text{ZRA},1}(r_0)$ coincides with the quantity $3E(r_0) - 4V_{\text{tr}}(r_0)$, i.e., formally Eq. (9) with $n_{\text{max}} = 1$ is equivalent to Eq. (5). It turns out, however, that our ECG implementation provides a more accurate estimate for $E^{(1)}(r_0)$ than for $V_{\text{tr}}(r_0)$. In Sec. III, we independently fit $E_{\text{ZRA},0}(r_0)$, $E_{\text{ZRA},1}(r_0)$, and $E_{\text{ZRA},2}(r_0)$ and compare the resulting zero-range energies. Appendix A shows that the functional forms of $E_{\text{ZRA},0}(r_0)$, $E_{\text{ZRA},1}(r_0)$, and $E_{\text{ZRA},2}(r_0)$ are correlated and presents the results of a single combined fit of $E_{\text{ZRA},0}(r_0)$, $E_{\text{ZRA},1}(r_0)$, and $E_{\text{ZRA},2}(r_0)$. The resulting zero-range energy is found to be consistent with the zero-range energies obtained from the independent fits.

The ECG calculations become numerically more challenging with decreasing two-body interaction range r_0 . The challenges arise from the need to resolve length scales of different orders of magnitude. In previous ECG calculations [21, 22], much effort was put on solving the Schrödinger equation for systems with small r_0 . In this work, we show that a reliable approximation to the zero-range energy can be obtained by calculating $E_{\text{ZRA},2}(r_0)$ at a range $r_0 \approx 0.1a_{\text{ho}}$. We demonstrate in Sec. III that $E_{\text{ZRA},1}(r_0)$ and $E_{\text{ZRA},2}(r_0)$ play important roles in obtaining the zero-range energy $E(0)$ and its errorbar.

To calculate the two-body Tan contact $C(r_0)$ at unitarity, we use the adiabatic energy relation [30],

$$C(r_0) = \frac{4\pi m}{\hbar^2} \left. \frac{\partial E(r_0)}{\partial(-a_s^{-1})} \right|_{a_s^{-1}=0}. \quad (11)$$

To obtain the two-body contact for $r_0 = 0$, we use the zeroth- and first-order zero-range extrapolation schemes, i.e., we extrapolate $C_{\text{ZRA},0}(r_0)$ and

$$C_{\text{ZRA},1}(r_0) = C(r_0) - \left. \frac{\partial C(\bar{r}_0)}{\partial \bar{r}_0} \right|_{\bar{r}_0 \rightarrow r_0} r_0 \quad (12)$$

to the zero-range limit.

The contact can alternatively be calculated through the pair relation

$$C(r_0) = N_1 \times N_2 \times \lim_{r \rightarrow 0, r \gg r_0} (4\pi)^2 P_{12}(r)r, \quad (13)$$

where $P_{12}(r)$ denotes the pair distribution function. The quantity $r^2 P_{12}(r)$ with normalization $4\pi \int_0^\infty P_{12}(r)r^2 dr = 1$ tells one the likelihood of finding two unlike particles at distance r from each other. The behavior of $4\pi P_{12}(r)r^2$ around $r \approx r_0$ depends on the details of the two-body interaction potential. Specifically, for finite-range potentials the quantity $4\pi P_{12}(r)r^2$ goes to zero as $r \rightarrow 0$. For the zero-range potential, in contrast, $4\pi P_{12}(r)r^2$ remains finite as $r \rightarrow 0$. Thus, to extract the finite-range contact via the pair relation, we consider the region where $r \gg r_0$ but $r \ll a_{\text{ho}}$. In practice, the condition $r \gg r_0$ translates to $r \gtrsim 2r_0$.

We also consider the spherically symmetric radial density $P_j(r)$ of species j , $j = 1$ and 2 . For even N ,

we have $P_1(r) = P_2(r)$. The quantity $P_j(r)$ tells one the likelihood of finding a particle at distance r from the trap center. The normalization is chosen such that $4\pi \int_0^\infty P_j(r)r^2 dr = 1$.

III. RESULTS

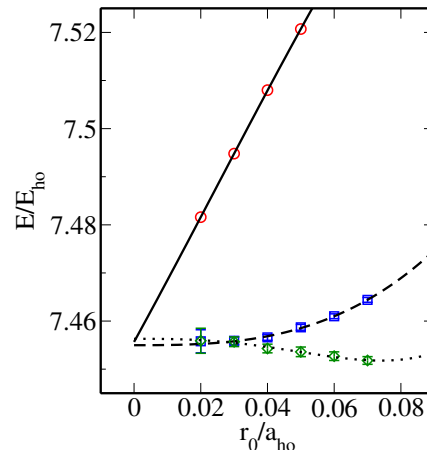


FIG. 2. (Color online) Ground state energy of the (3,2) system at unitarity as a function of r_0 . Circles, squares, and diamonds show the energies $E_{\text{ZRA},0}(r_0)$, $E_{\text{ZRA},1}(r_0)$, and $E_{\text{ZRA},2}(r_0)$, respectively, reported in the last three columns of Table I. The uncertainty of $\Delta E(r_0)$ is not accounted for by the errorbars. Solid, dashed, and dotted lines show polynomial fits to $E_{\text{ZRA},0}(r_0)$, $E_{\text{ZRA},1}(r_0)$, and $E_{\text{ZRA},2}(r_0)$.

This section discusses the energies and other observables of the systems with $N \leq 10$ obtained by the ECG method. We use the (3,2) system to explain our new range correction scheme. Column 2 of Table I shows the finite-range energies $E(r_0)$ obtained by the ECG approach for various two-body interaction ranges r_0 . The reported energies are obtained for the largest basis set considered. They provide variational upper bounds for the finite-range Hamiltonian with Gaussian interaction. Column 3 reports the estimated basis set error $\Delta E(r_0)$. For all r_0 considered, the basis set error is less than 0.02%. Columns 4 and 5 show the quantities $E^{(1)}(r_0)$ and $E^{(2)}(r_0)$, respectively. While $E^{(1)}(r_0)$ increases slightly with decreasing range r_0 , this increase is smaller than the decrease of r_0 , implying that the range correction $E^{(1)}(r_0)r_0$ decreases with decreasing r_0 . The magnitude of $E^{(2)}(r_0)$ decreases with decreasing r_0 . Note that we are not able to estimate $E^{(2)}(r_0)$ reliably for small r_0 (the errorbars are larger than the quantity itself). Yet, the errorbars of $E^{(2)}(r_0)$ allow us to estimate the maximal correction proportional to r_0^2 for each r_0 , thereby providing us with another means to estimate errorbars. Columns 6-8 of Table I show $E_{\text{ZRA},j}(r_0)$ with $j = 0, 1$, and 2 . These values are obtained by subtracting the basis set error $\Delta E(r_0)$. The leading-order range dependence of $E_{\text{ZRA},0}(r_0)$ is linear and we perform a fit of the

TABLE I. Ground state energy of the (3,2) system at unitarity. Column 2 shows the finite-range energy for the largest basis set considered. The estimated basis set error $\Delta E(r_0)$ is reported in column 3. Columns 4 and 5 report the quantities $E^{(1)}(r_0)$ and $E^{(2)}(r_0)$; errorbars are given in parenthesis. The energy derivatives are calculated for the largest basis set considered. Columns 6-8 report the energies $E_{\text{ZRA},0}(r_0)$, $E_{\text{ZRA},1}(r_0)$, and $E_{\text{ZRA},2}(r_0)$. These energies account for the estimated basis set extrapolation error, i.e., $E(r_0) - \Delta E(r_0)$ is being used to calculate $E_{\text{ZRA},j}(r_0)$ for $j = 0, 1$, and 2. The errorbars of $E_{\text{ZRA},1}(r_0)$ and $E_{\text{ZRA},2}(r_0)$ account for the uncertainties of $E^{(1)}(r_0)$ and $E^{(2)}(r_0)$ but do not account for the uncertainty of $\Delta E(r_0)$. The last row reports the extrapolation of $E_{\text{ZRA},j}(r_0)$ to the zero-range limit.

$\frac{r_0}{a_{\text{ho}}}$	$\frac{E(r_0)}{E_{\text{ho}}}$	$\frac{\Delta E(r_0)}{E_{\text{ho}}}$	$E^{(1)}(r_0) \frac{a_{\text{ho}}}{E_{\text{ho}}}$	$E^{(2)}(r_0) \frac{a_{\text{ho}}^2}{E_{\text{ho}}}$	$\frac{E_{\text{ZRA},0}(r_0)}{E_{\text{ho}}}$	$\frac{E_{\text{ZRA},1}(r_0)}{E_{\text{ho}}}$	$\frac{E_{\text{ZRA},2}(r_0)}{E_{\text{ho}}}$
0.07	7.5449	0.0001	1.148(7)	-5.13(12)	7.5448	7.4644(5)	7.4518(8)
0.06	7.5332	0.0001	1.201(8)	-4.61(25)	7.5331	7.4610(5)	7.4527(9)
0.05	7.5211	0.0004	1.240(12)	-4.11(28)	7.5207	7.4587(6)	7.4536(10)
0.04	7.5084	0.0004	1.284(15)	-2.85(33)	7.5080	7.4566(6)	7.4543(9)
0.03	7.4954	0.0006	1.297(26)	-0.32(46)	7.4948	7.4559(8)	7.4557(10)
0.02	7.4825	0.0009	1.290(120)	0.24(96)	7.4816	7.4558(24)	7.4559(26)
0					7.4557	7.4550	7.4563

form $c_0 + c_1 r_0 + c_2 r_0^2 + c_3 r_0^3$. The extrapolated zero-range energy is reported in the last row of column 6. The leading order range dependence of $E_{\text{ZRA},1}(r_0)$ is quadratic and we perform a fit of the form $c_0 + c_2 r_0^2 + c_3 r_0^3 + c_4 r_0^4$, weighted by the inverse square of the uncertainty. The extrapolated zero-range energy is reported in the last row of column 7. The leading-order range dependence of $E_{\text{ZRA},2}(r_0)$ is cubic and we perform a fit of the form $c_0 + c_3 r_0^3 + c_4 r_0^4$, weighted by the inverse square of the uncertainty. The extrapolated zero-range energy is reported in the last row of column 8. Table I shows that the zeroth-, first- and second-order extrapolation schemes yield zero-range energies that differ by at most $0.0013E_{\text{ho}}$. This confirms that the range-dependence of the (3,2) ground state energy for the r_0 considered is well described by a Taylor series. Moreover, we note that $E_{\text{ZRA},2}(r_0)$ for $r_0 = 0.07a_{\text{ho}}$ differs by only $0.0045E_{\text{ho}}$ from the extrapolated zero-range energy. This suggests that $E_{\text{ZRA},2}(r_0)$ obtained at a single (relatively large) range provides a very good estimate for the zero-range energy. Circles, squares, and diamonds in Fig. 2 show the energies $E_{\text{ZRA},0}(r_0)$, $E_{\text{ZRA},1}(r_0)$, and $E_{\text{ZRA},2}(r_0)$, respectively. The fits (see the discussion above) are shown by lines.

For systems with up to six particles (see the Supplemental Material [27] for a summary), we believe that our basis sets for all r_0 are very close to complete. Specifically, (i) the energy changes very little upon further enlargement of the basis set, (ii) the first- and second-order derivatives $E^{(1)}(r_0)$ and $E^{(2)}(r_0)$ are stable and their errorbars can be estimated reliably, (iii) the extrapolations of $E_{\text{ZRA},0}(r_0)$, $E_{\text{ZRA},1}(r_0)$, and $E_{\text{ZRA},2}(r_0)$ are in very good agreement, and (iv) the quantities $3E(r_0) - 4V_{\text{tr}}(r_0)$ and $E_{\text{ZRA},1}(r_0)$ agree quite well [see the discussion after Eq. (10)]. For systems with more than six particles, the construction of a nearly complete basis set is more challenging, especially for small r_0 . As an example, we discuss the (4,4) system; for the (4,3), (5,4), and (5,5) systems, the reader is referred to the Supplemental Material [27].

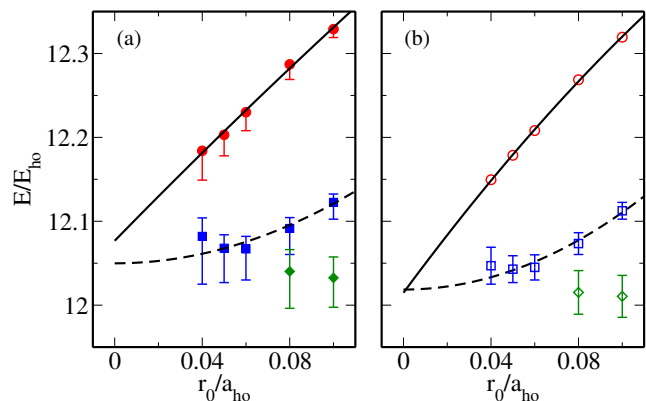


FIG. 3. (Color online) Ground state energy of the (4,4) system at unitarity. (a) Circles, squares, and diamonds show $E_{\text{ZRA},0}(r_0)$, $E_{\text{ZRA},1}(r_0)$, and $E_{\text{ZRA},2}(r_0)$, respectively, for the largest basis set considered. The errorbars of $E_{\text{ZRA},0}(r_0)$ show the estimated basis set error $\Delta E(r_0)$ (see column 3 of Table II); they extend below the data points but not above. The errorbars of $E_{\text{ZRA},1}(r_0)$ combine the estimated basis set error and the error of $E^{(1)}(r_0)$ (see column 4 of Table II). Lastly, the errorbars of $E_{\text{ZRA},2}(r_0)$ combine the estimated basis set error, and the errors of $E^{(1)}(r_0)$ and $E^{(2)}(r_0)$ (see column 5 of Table II). Solid and dashed lines show the extrapolations of $E_{\text{ZRA},0}(r_0)$ and $E_{\text{ZRA},1}(r_0)$ to the zero-range limit. (b) Same quantities as in (a) but corrected for the estimated basis set errors. The open symbols show the energies $E_{\text{ZRA},0}(r_0)$, $E_{\text{ZRA},1}(r_0)$, and $E_{\text{ZRA},2}(r_0)$ reported in the last three columns of Table II. The uncertainty of $\Delta E(r_0)$ is not accounted for by the errorbars. It can be seen that the basis set error lowers the zero-range energy by about $0.05E_{\text{ho}}$ or, equivalently, 0.4%.

Table II summarizes our ECG results for the (4,4) system; the format is the same as that in Table I for the (3,2) system. The smallest range considered and the errorbars for the $N = 8$ system are larger than those for the $N = 5$ system. For a fixed r_0 , the quantities $E^{(1)}(r_0)$ and $E^{(2)}(r_0)$ for the $N = 8$ system are about twice as large as for the $N = 5$ system and their er-

TABLE II. Same as Table I but for the (4,4) system at unitarity.

$\frac{r_0}{a_{\text{ho}}}$	$\frac{E(r_0)}{E_{\text{ho}}}$	$\frac{\Delta E(r_0)}{E_{\text{ho}}}$	$E^{(1)}(r_0) \frac{a_{\text{ho}}}{E_{\text{ho}}}$	$E^{(2)}(r_0) \frac{a_{\text{ho}}^2}{E_{\text{ho}}}$	$\frac{E_{\text{ZRA},0}(r_0)}{E_{\text{ho}}}$	$\frac{E_{\text{ZRA},1}(r_0)}{E_{\text{ho}}}$	$\frac{E_{\text{ZRA},2}(r_0)}{E_{\text{ho}}}$
0.1	12.329	0.010	2.07(10)	-18(3)	12.319	12.113(10)	12.011(25)
0.08	12.287	0.018	2.44(16)	-16(4)	12.269	12.073(13)	12.015(26)
0.06	12.230	0.022	2.72(25)		12.208	12.045(15)	
0.05	12.204	0.025	2.71(32)		12.179	12.043(16)	
0.04	12.184	0.035	2.56(55)		12.149	12.047(22)	
0					12.015	12.019	

rorbars are notably larger. The overall trends, however, are similar: (i) the energy $E(r_0)$ decreases with decreasing range, (ii) $E^{(1)}(r_0)$ increases with decreasing range for $r_0 \geq 0.06a_{\text{ho}}$ (for smaller r_0 , the trend reverses; we believe that this is a consequence of the numerics and not a real trend), and (iii) $E^{(2)}(r_0)$ becomes less negative with decreasing range. Our numerics are not good enough to determine $E^{(2)}(r_0)$ for $r_0 \leq 0.06a_{\text{ho}}$. It can be seen, however, that the $E_{\text{ZRA},2}(r_0)$ for $r_0 = 0.1a_{\text{ho}}$ and $0.08a_{\text{ho}}$ agree quite well with the energies obtained by extrapolating $E_{\text{ZRA},0}(r_0)$ and $E_{\text{ZRA},1}(r_0)$ to the zero-range limit (see the last row of Table II). Since the basis set error is non-negligible for $N = 8$, Fig. 3 shows the energies $E_{\text{ZRA},0}(r_0)$ (circles), $E_{\text{ZRA},1}(r_0)$ (squares), and $E_{\text{ZRA},2}(r_0)$ (diamonds) before correcting for the basis set error [Fig. 3(a)] and after correcting for the basis set error [Fig. 3(b)]. We extrapolate $E_{\text{ZRA},0}(r_0)$ and $E_{\text{ZRA},1}(r_0)$ for both the largest basis set considered [Fig. 3(a)] and the infinite basis set [Fig. 3(b)] to the zero-range limit by performing fits of the form $c_0 + c_1r_0 + c_2r_0^2$ and $c_0 + c_2r_0^2$, respectively (see solid and dashed lines in Fig. 3). To fit a function to $E_{\text{ZRA},1}(r_0)$, the data points are weighted by the inverse square of the uncertainty. For the (4,4) and larger systems, we do not fit to higher-order polynomials because (i) the number of data points is five or less and (ii) the errorbars are too large to determine the r_0^3 dependence reliably. An alternative fit approach that includes the r_0^3 term is discussed in Appendix A.

Table III summarizes our zero-range ground state energies $E(0)$ (column 2) obtained by extrapolating the energies $E_{\text{ZRA},1}(r_0)$, which have been shifted down by the estimated basis set error, to the zero-range limit. The errorbars given in parenthesis are estimated by combining the zero-range extrapolation error, the uncertainty of the basis set error, and the uncertainty of $E^{(1)}(r_0)$.

Our ground state energy for the (2,1) system agrees excellently with the semi-analytic energy obtained using the zero-range framework of Ref. [31]. For comparison, Table III includes the ground state energies from the literature obtained by various methods. Column 3 of Table III reports the zero-range ground state energies E_{ECG} calculated by the ECG method in previous works [18, 20, 23]. Our results for the (2,2), (3,2) and (3,3) systems agree within errorbars with the literature results. For the (3,3) system, we provide a notably tighter errorbar. The ECG energy for the (4,4) system by Bradly *et al.* [23] is about 0.9% higher than our (4,4) energy. Bradly *et al.* esti-

mate that the error due to the use of a restricted basis set is about 0.6% for the relative energy, translating to 0.53% for the total energy. This estimate is in reasonable agreement with the difference between their energy and our energy. Column 5 reports the FN-DMC energies E_{DMC1} calculated for the square well potential with range $0.01a_{\text{ho}}$ [7]. The deviations between the FN-DMC and our ECG energies are due to the positive effective range correction and the approximate nature of the nodal surface of the trial wave function (the latter dominates). Column 7 reports highly-improved FN-DMC energies E_{DMC2} [12]. These energies have been extrapolated to the zero-range limit. The FN-DMC energies from Ref. [12] agree very well with our ECG energies (the agreement is better than 0.6% and, for $N = 8$ and 10, the errorbars overlap). Unfortunately, Ref. [12] considered only spin-balanced systems. Columns 9 and 11 report the energies E_{AFMC2} and E_{AFMC4} calculated using the AFMC approach with q^2 and $q^2 + q^4$ dispersion relations, respectively [12]. These energies have been obtained by applying a leading-order correction scheme to convert the finite lattice results to the infinite lattice limit but have not been extrapolated to the infinite lattice size limit [12, 32]. Note that the AFMC energies for fixed N but different dispersion relations do not agree within errorbars. The reason may be that the corrections due to the finite lattice spacing behave differently for the different dispersion relations and that the errorbars are purely statistical. Column 13 reports the configuration interaction (CI) energies E_{CI} obtained using a limited CI shell model space [13]. The authors of Ref. [13] noted that the two-body interaction strength was renormalized using an approach that could be improved upon. Improvement to both these aspects (enlarged CI model space and refined renormalization approach) could change the CI energies. Interestingly, the odd N CI energies agree quite well with our ECG energies while the even N CI energies are higher by between 1.3% and 3.2%. It is not clear to us what the origin of the different even and odd N behaviors is. Column 15 reports the lattice MC energies E_{lattice} [10]. The lattice MC energies exhibit shell effects that are absent in the FN-DMC, AFMC, and—for small N —ECG energies (our energies for $N \leq 10$ do not exhibit shell effects). The lattice MC energy for $N = 8$ is 3.2% lower than our ECG, reflecting the shell effects exhibited by the lattice MC energies in the small N regime. For systems with $N > 10$, the lattice MC energies are higher than or equal

TABLE III. Summary of our zero-range ground state energies at unitarity and comparison with literature results for systems with $N \leq 10$ and $N_1 - N_2 \leq 1$. Column 2 reports the zero-range ground state energies $E(0)$ calculated in this work. Columns 3 to 16 report ground state energies from the literature calculated by different methods and their percentage differences from $E(0)$. All energies are reported in units of E_{ho} . The ground state energy of the (2,1) system, obtained semi-analytically [31], is $4.272724E_{\text{ho}}$. See text for more details.

(N_1, N_2)	$E(0)$	E_{ECG}	%	$E_{\text{DMC1}}^{\text{a}}$	%	$E_{\text{DMC2}}^{\text{b}}$	%	$E_{\text{AFMC2}}^{\text{c}}$	%	$E_{\text{AFMC4}}^{\text{c}}$	%	E_{CI}^{d}	%	$E_{\text{lattice}}^{\text{e}}$	%
(2,1)	4.2727(1)			4.281(4)	0.2							4.279	0.1		
(2,2)	5.0091(4)	5.0092(4) ^f		5.051(9)	0.8	5.028(2)	0.4					5.138	2.6	5.071(+32/-75)	1.2
(3,2)	7.455(1)	7.457(3) ^g		7.61(1)	2.1										
(3,3)	8.337(4)	8.34(9) ^g		8.64(3)	3.6	8.377(3)	0.5	8.26(1)	-0.9	8.21(1)	-1.6	8.601	3.2	8.347(+80/-66)	0.1
(4,3)	11.01(2)			11.36(2)	3.2							11.021	0.1		
(4,4)	12.02(3)	12.13(1) ^h	0.9	12.58(3)	4.7	12.04(1)	0.2	11.82(2)	-1.7	11.76(3)	-2.2	12.179	1.3	11.64(+11/-12)	-3.2
(5,4)	15.24(9)			15.69(1)	3.0										
(5,5)	16.12(6)			16.80(4)	4.2	16.10(1)	-0.1							16.05(+3/-7)	-0.4

^a From Table II of Ref. [7]; the energies have been calculated for the square well potential with range $r_0 = 0.01a_{\text{ho}}$, corresponding to $r_{\text{eff}} = 0.01a_{\text{ho}}$.

^b Read off from Fig. 4 of Ref. [12]; the FN-DMC energies have been extrapolated to the zero-range limit.

^c Read off from Fig. 4 of Ref. [12]; the errorbars only account for the statistical uncertainty. A leading-order correction scheme has been applied to convert the finite lattice results to the infinite lattice limit [12, 32].

^d From Table I of Ref. [13]; the CI energies have been obtained for a finite shell model space and the two-body coupling constant has been renormalized by matching the two-particle ground state energy to the exact energy.

^e From Table VI of Ref. [10]; the upper and lower limits of the errorbars are different and separated by a slash. The errorbars account for statistical, fitting, finite volume, and spatial discretization errors, but do not account for systematic errors due to the contributions from excited states. We note that odd N systems were considered in Ref. [9]. The results in Ref. [9] were described as “preliminary” and are not included here.

^f From Ref. [20]; the energy has been obtained by solving the hyperangular Schrödinger equation.

^g From Table XXI of Ref. [18]; the energies have been extrapolated to the zero-range limit using the zeroth-order extrapolation scheme.

^h From Table II of Ref. [23]; the energy has been extrapolated to the zero-range limit using the zeroth-order extrapolation scheme.

to (within errorbars) the FN-DMC energies E_{DMC2} from Ref. [12]. The difference between the lattice MC energies and FN-DMC energies for $N > 10$ is smallest for closed shell systems. Besides the results summarized in Table III, we also compared our ground state energies with DFT energies [14] for both even and odd N systems. The DFT energies are 5% to 10% higher than our ECG energies.

TABLE IV. Zero-range contact $C(0)$ at unitarity for $N = 3 - 10$. Column 2 reports the zero-range contact $C(0)$ determined using the adiabatic energy relation. $C(0)$ for the (1,1) system, obtained analytically from the implicit eigenequation derived in Ref. [33], is $4\sqrt{2\pi}a_{\text{ho}}^{-1} = 10.026513a_{\text{ho}}^{-1}$. $C(0)$ for the (2,1) system, obtained semi-analytically using the hyperspherical coordinate framework [31, 34, 35], is $10.468967a_{\text{ho}}^{-1}$.

(N_1, N_2)	$C(0)a_{\text{ho}}$
(2,1)	10.469(1)
(2,2)	25.74(1)
(3,2)	25.20(1)
(3,3)	40.39(8)
(3,4)	38.2(2)
(4,4)	55.4(5)
(5,4)	56.9(9)
(5,5)	72.3(8)

In addition to the energies, we calculate the contact at unitarity. To remove the leading-order range dependence, we analyze the quantities $C_{\text{ZRA},0}(r_0)$ and $C_{\text{ZRA},1}(r_0)$.

While the energies $E_{\text{ZRA},0}(r_0)$ and $E_{\text{ZRA},1}(r_0)$ approach the $r_0 = 0$ limit from above and below, respectively, for all N considered, the contacts $C_{\text{ZRA},0}(r_0)$ and $C_{\text{ZRA},1}(r_0)$ approach the $r_0 = 0$ limit from either above or below. Specifically, fitting $C_{\text{ZRA},0}(r_0)$ to a function of the form $c_0 + c_1r_0 + c_2r_0^2$, we find that c_1 is positive for $N = 4$, very close to zero for $N = 6$, negative for $N = 8$, and again positive for $N = 10$. For the odd N systems, c_1 is always positive. The pair distribution functions exhibit an analogous range-dependence in the $r_0 \ll r \ll a_{\text{ho}}$ region (see Figs. 9 and 10 of the Supplemental Material for the $N = 5$ and 8 systems), suggesting that the intricate N and r_0 dependence of the contact is a real effect and not an artifact of our numerics. Our convergence studies support this interpretation. Table IV reports the zero-range contact $C(0)$ for $N = 3 - 10$ at unitarity obtained by extrapolating $C_{\text{ZRA},1}(r_0)$ to the zero-range limit. The errorbars in parenthesis account for the zero-range extrapolation error and the basis set error. The $r_0 = 0$ extrapolations of $C_{\text{ZRA},0}(r_0)$ and of the contact extracted from the pair distribution functions agree with the values reported in Table IV but have larger errorbars. The contact exhibits an interesting even-odd pattern. Specifically, for the $N = 4$ and 5 systems (and the 6 and 7 systems, and the 8 and 9 systems), the contacts are roughly equal, reflecting the fact that these neighboring even-odd systems contain the same number of pairs. To zeroth-order, the contact scales as N_2 times the contact of the two-body system, i.e., linearly with the number of

pairs. Since $C(0)$ scales with N_2 , the $r_0 \ll r \ll a_{\text{ho}}$ region of the scaled pair distribution functions $4\pi P_{12}(r)r^2$ approximately collapse to a single curve if multiplied by N_1 . This approximate collapse is illustrated in Figs. 4(c) and 4(d).

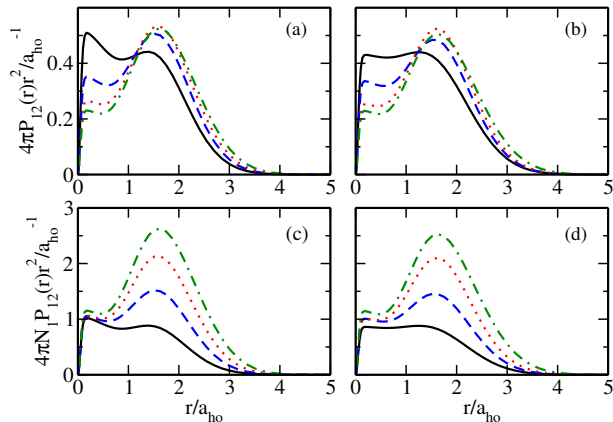


FIG. 4. (Color online) Panels (a) and (c) show the scaled pair distribution functions $4\pi P_{12}(r)r^2$ and $4\pi N_1 P_{12}(r)r^2$, respectively, of the ground state at unitarity for the (2,2) system (solid line), (3,3) system (dashed line), (4,4) system (dotted line), and (5,5) system (dash-dotted line). Panels (b) and (d) show the scaled pair distribution functions $4\pi P_{12}(r)r^2$ and $4\pi N_1 P_{12}(r)r^2$, respectively, of the ground state at unitarity for the (2,1) system (solid line), (3,2) system (dashed line), (4,3) system (dotted line), and (5,4) system (dash-dotted line). The calculations are performed for $r_0 = 0.06a_{\text{ho}}$.

Figure 5 shows the radial density $P_1(r)$ of the ground state at unitarity for even N and $r_0 = 0.06a_{\text{ho}}$. We note that the convergence of the radial density in the small r regime is not as good as that of the pair distribution function, especially for large N and small r_0 . $P_1(r)$ peaks at $r = 0$ for the (2,2) system, is relatively flat in the small r region for the (3,3) and (5,5) systems, and peaks around $0.6a_{\text{ho}}$ for the (4,4) system. To estimate the range dependence, we calculate $P_1(r)$ for different r_0 for the (2,2), (3,3), and (4,4) systems. For a given system, the $r \gtrsim 0.5a_{\text{ho}}$ region of $P_1(r)$ increases with decreasing two-body range r_0 (see Fig. 8 of the Supplemental Material [27]). The changes with r_0 are relatively small and the densities displayed in Fig. 5 show the generic behavior of trapped Fermi gases with short-range interactions. Figure 6 shows $P_j(r)$, $j = 1$ and 2, for the odd N systems at unitarity for $r_0 = 0.06a_{\text{ho}}$. $P_1(r)$ and $P_2(r)$ peak at $r = 0$ for the (2,1) system, are relatively flat in the small r region for the (3,2) and (5,4) systems, and peak around $0.5a_{\text{ho}}$ for the (4,3) system. We find that the range-dependence of the radial density for the odd N systems is similar to that for the even N systems (see Fig. 7 of the Supplemental Material [27]).

To gain insights into the pairing of the particles, Fig. 7 shows the integrated quantities $\bar{N}_j(r)$,

$$\bar{N}_j(r) = 4\pi N_j \int_0^r P_j(r') r'^2 dr', \quad (14)$$

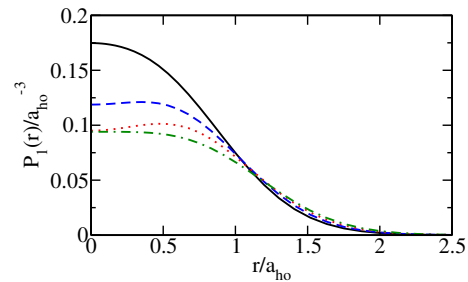


FIG. 5. (Color online) Radial density $P_1(r)$ of the ground state at unitarity for the (2,2) system (solid line), (3,3) system (dashed line), (4,4) system (dotted line), and (5,5) system (dash-dotted line). The calculations are performed for $r_0 = 0.06a_{\text{ho}}$.

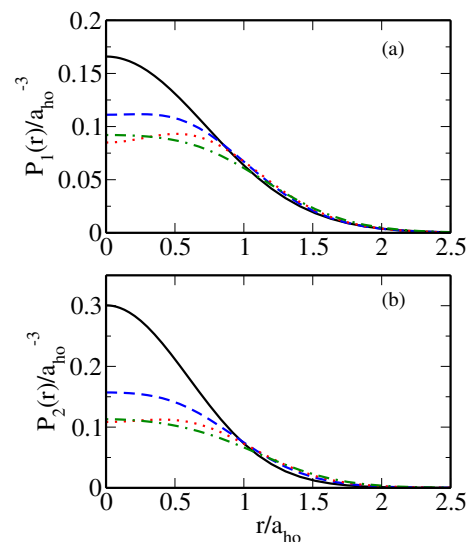


FIG. 6. (Color online) Panels (a) and (b) show the radial density of the majority species $P_1(r)$ and the minority species $P_2(r)$, respectively, for the ground state of the (2,1) system (solid line), (3,2) system (dashed line), (4,3) system (dotted line), and (5,4) system (dash-dotted line). The calculations are performed for $r_0 = 0.06a_{\text{ho}}$.

for the odd N systems. Solid and dashed lines show $\bar{N}_j(r)$ for the majority ($j = 1$) and minority ($j = 2$) species, respectively. $\bar{N}_j(r)$ monitors the number of particles of species j located between zero and r , and approaches N_j in the large r limit. We find that $\bar{N}_1(r)$ and $\bar{N}_2(r)$ take, for N fixed, different values for all r , suggesting that there exists no core region where the systems are fully paired. This is in contrast to an earlier FN-DMC study [8], which suggested that the $N = 9$ system has a fully paired core. It should be noted that a fully paired core is expected in the large N limit [36]; however, how many particles are needed to be in the large N limit is not clear.

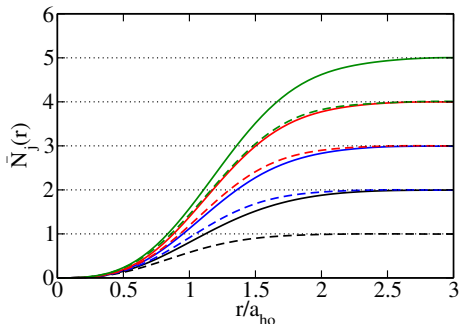


FIG. 7. (Color online) Solid and dashed lines show the integrated quantities $\bar{N}_1(r)$ and $\bar{N}_2(r)$, respectively, for odd N systems as a function of r . From bottom to top, the curves correspond to systems with $N = 3, 5, 7$, and 9 . The horizontal dotted lines at 1 to 5 serve as a guide to the eye. The calculations are performed for $r_0 = 0.06a_{\text{ho}}$.

IV. CONCLUSIONS

This paper considered the ground state properties of trapped two-component Fermi gases at unitarity with up to ten particles. The calculations were performed for interspecies finite-range Gaussian interaction potentials using the ECG approach. Previous ECG calculations were limited to $N = 3 - 6$ and 8 . The present work additionally considered the spin-imbalanced $N = 7$ and 9 systems with $L^\pi = 1^-$ symmetry and the spin-balanced $N = 10$ system with $L^\pi = 0^+$ symmetry. A new range-correction scheme, which allows for the leading and—in some cases—the sub-leading range dependence to be removed, was introduced. The accuracy of the range correction scheme was tested extensively for small N systems ($N \leq 6$) and then applied to larger systems ($N = 7 - 10$). The resulting extrapolated zero-range energies have errorbars that range from 0.002% for $N = 3$ to 0.6% and 0.4% for $N = 9$ and 10 . The energies agree well with the FN-DMC energies from Ref. [12], suggesting that the zero-range energies of harmonically trapped two-component Fermi gases with $N \leq 10$ ($N_1 - N_2 = 0$ or 1) are now known with an accuracy better than 1%. The finite-range energies were reported for finite r_0 and all N . These finite-range energies provide variational upper bounds and are expected to help assess the accuracy of future finite-range calculations (the range r_0 can be easily converted to the effective range). In addition to the energy, the pair distribution functions and radial densities were analyzed. The Tan contacts obtained through the adiabatic and pair relations were found to agree within errorbars.

V. ACKNOWLEDGEMENTS

We gratefully acknowledge discussions with Y. Yan, Y. Alhassid, and M. M. Forbes, email correspondence with J. Carlson, and support by the National Science Founda-

tion (NSF) through Grant No. PHY-1205443. This work used the Extreme Science and Engineering Discovery Environment (XSEDE), which is supported by NSF Grant No. ACI-1053575, and the WSU HPC.

Appendix A: Additional comments on the range-correction scheme

In the main text, we independently fit the quantities $E_{\text{ZRA},0}(r_0)$, $E_{\text{ZRA},1}(r_0)$, and $E_{\text{ZRA},2}(r_0)$. The resulting zero-range energies were found to be in good agreement. This appendix discusses that a single correlated fit yields results that are consistent with those obtained from the independent fits.

We assume that the ground state energy $E(r_0) = E_{\text{ZRA},0}(r_0)$ is a polynomial in the two-body interaction range r_0 ,

$$E(r_0) = c_0 + c_1 r_0 + c_2 r_0^2 + c_3 r_0^3 + \mathcal{O}(r_0^4). \quad (\text{A1})$$

Using Eq. (A1) to calculate $E^{(1)}(r_0)$ and $E^{(2)}(r_0)$ and inserting the results into Eq. (10), we find

$$E_{\text{ZRA},1}(r_0) = c_0 - c_2 r_0^2 - 2c_3 r_0^3 + \mathcal{O}(r_0^4) \quad (\text{A2})$$

and

$$E_{\text{ZRA},2}(r_0) = c_0 + c_3 r_0^3 + \mathcal{O}(r_0^4). \quad (\text{A3})$$

As expected, the leading-order range-dependencies of $E_{\text{ZRA},1}(r_0)$ and $E_{\text{ZRA},2}(r_0)$ are quadratic and cubic, respectively, and the functional forms of $E_{\text{ZRA},j}(r_0)$ are not independent. Specifically, the quadratic coefficient of $E_{\text{ZRA},1}(r_0)$ has the opposite sign but the same magnitude as that of $E_{\text{ZRA},0}(r_0)$, the cubic coefficient of $E_{\text{ZRA},1}(r_0)$ has the opposite sign but twice the magnitude as that of $E_{\text{ZRA},0}(r_0)$, and the cubic coefficient of $E_{\text{ZRA},2}(r_0)$ is the same as that of $E_{\text{ZRA},0}(r_0)$. Interestingly, our independent fits shown in Figs. 2 and 3 of the main text and Figs. 1-6 of the Supplemental Material are largely consistent with Eqs. (A1)-(A3). For example, our fits of $E_{\text{ZRA},0}(r_0)$ yield a negative r_0^2 coefficient and those of $E_{\text{ZRA},1}(r_0)$ yield a positive r_0^2 coefficient. The magnitudes of these coefficients, however, depend fairly sensitively on the number of terms included in the independent fits.

As an alternative, we perform a simultaneous four-parameter fit of $E_{\text{ZRA},0}(r_0)$, $E_{\text{ZRA},1}(r_0)$, and $E_{\text{ZRA},2}(r_0)$ using Eqs. (A1)-(A3). Each data point is weighted by the inverse square of the uncertainty [for $E_{\text{ZRA},0}(r_0)$ we assume an uncertainty of $0.3\Delta E(r_0)$ and the uncertainties of $E_{\text{ZRA},1}(r_0)$ and $E_{\text{ZRA},2}(r_0)$ are given in Tables I and II of the main text and Tables I-VI of the Supplemental Material]. The resulting zero-range energies for $N = 3 - 10$ are $4.2726E_{\text{ho}}$, $5.0088E_{\text{ho}}$, $7.454E_{\text{ho}}$, $8.335E_{\text{ho}}$, $11.01E_{\text{ho}}$, $12.02E_{\text{ho}}$, $15.25E_{\text{ho}}$, and $16.12E_{\text{ho}}$, respectively. These energies lie within the errorbars of the zero-range energies reported in Table III. The simultaneous fit yields a positive c_1 coefficient and negative c_2 and c_3 coefficients

for all N . The c_1 coefficient obtained from the independent fit of $E_{\text{ZRA},0}(r_0)$ differs from that obtained from the simultaneous fit by less than 10% for all N .

We also apply the simultaneous fit approach to the contact. We fit our numerically obtained $C_{\text{ZRA},0}(r_0)$ and

$C_{\text{ZRA},1}(r_0)$ to functions of the form $c_0 + c_1r_0 + c_2r_0^2 + c_3r_0^3$ and $c_0 - c_2r_0^2 - 2c_3r_0^3$, respectively, for $N < 6$, and to functions of the form $c_0 + c_1r_0 + c_2r_0^2$ and $c_0 - c_2r_0^2$, respectively, for $N = 7 - 10$. The resulting zero-range contacts $C(0)$ for $N = 3 - 10$ lie within the errorbars of the zero-range contacts reported in Table IV.

-
- [1] S. Giorgini, L. P. Pitaevskii, and S. Stringari, “Theory of ultracold atomic Fermi gases,” *Rev. Mod. Phys.* **80**, 1215 (2008).
- [2] D. Blume, “Few-body physics with ultracold atomic and molecular systems in traps,” *Reports on Progress in Physics* **75**, 046401 (2012).
- [3] A. Gezerlis and J. Carlson, “Strongly paired fermions: Cold atoms and neutron matter,” *Phys. Rev. C* **77**, 032801 (2008).
- [4] A. G. Truscott, K. E. Strecker, W. I. McAlexander, G. B. Partridge, and R. G. Hulet, “Observation of Fermi pressure in a gas of trapped atoms,” *Science* **291**, 2570 (2001).
- [5] B. DeMarco and D. S. Jin, “Onset of Fermi degeneracy in a trapped atomic gas,” *Science* **285**, 1703 (1999).
- [6] S. Y. Chang and G. F. Bertsch, “Unitary Fermi gas in a harmonic trap,” *Phys. Rev. A* **76**, 021603 (2007).
- [7] D. Blume, J. von Stecher, and C. H. Greene, “Universal properties of a trapped two-component Fermi gas at unitarity,” *Phys. Rev. Lett.* **99**, 233201 (2007).
- [8] J. von Stecher, C. H. Greene, and D. Blume, “Energetics and structural properties of trapped two-component Fermi gases,” *Phys. Rev. A* **77**, 043619 (2008).
- [9] A. N. Nicholson, M. G. Endres, D. B. Kaplan, and J.-W. Lee, “Lattice study of trapped fermions at unitarity,” In proceedings of the XXVIII International Symposium on Lattice Field Theory (Lattice 2010), Villasimius, Italy, June 14-19, 2010. See also arXiv:1011.2804.
- [10] M. G. Endres, D. B. Kaplan, J.-W. Lee, and A. N. Nicholson, “Lattice Monte Carlo calculations for unitary fermions in a harmonic trap,” *Phys. Rev. A* **84**, 043644 (2011).
- [11] M. M. Forbes, S. Gandolfi, and A. Gezerlis, “Effective-range dependence of resonantly interacting fermions,” *Phys. Rev. A* **86**, 053603 (2012).
- [12] J. Carlson and S. Gandolfi, “Predicting energies of small clusters from the inhomogeneous unitary Fermi gas,” *Phys. Rev. A* **90**, 011601(R) (2014).
- [13] A. Mukherjee and Y. Alhassid, “Configuration-interaction Monte Carlo method and its application to the trapped unitary Fermi gas,” *Phys. Rev. A* **88**, 053622 (2013).
- [14] A. Bulgac, “Local-density-functional theory for superfluid fermionic systems: The unitary gas,” *Phys. Rev. A* **76**, 040502(R) (2007).
- [15] L. Salasnich and F. Toigo, “Extended Thomas-Fermi density functional for the unitary Fermi gas,” *Phys. Rev. A* **78**, 053626 (2008).
- [16] S. K. Adhikari and L. Salasnich, “Effective nonlinear Schrödinger equations for cigar-shaped and disc-shaped Fermi superfluids at unitarity,” *New Journal of Physics* **11**, 023011 (2009).
- [17] S. K. Adhikari, “Universal behavior of a trapped Fermi superfluid in the BCS-unitarity crossover,” *Phys. Rev. A* **79**, 023611 (2009).
- [18] J. Mitroy, S. Bubin, W. Horiuchi, Y. Suzuki, L. Adamowicz, W. Cencek, K. Szalewicz, J. Komasa, D. Blume, and K. Varga, “Theory and application of explicitly correlated Gaussians,” *Rev. Mod. Phys.* **85**, 693 (2013).
- [19] D. Blume and K. M. Daily, “Universal relations for a trapped four-fermion system with arbitrary s -wave scattering length,” *Phys. Rev. A* **80**, 053626 (2009).
- [20] J. von Stecher and C. H. Greene, “Correlated Gaussian hyperspherical method for few-body systems,” *Phys. Rev. A* **80**, 022504 (2009).
- [21] D. Blume and K. M. Daily, “Trapped two-component Fermi gases with up to six particles: Energetics, structural properties, and molecular condensate fraction,” *Comptes Rendus Physique* **12**, 86 (2011).
- [22] D. Rakshit, K. M. Daily, and D. Blume, “Natural and unnatural parity states of small trapped equal-mass two-component Fermi gases at unitarity and fourth-order virial coefficient,” *Phys. Rev. A* **85**, 033634 (2012).
- [23] C. J. Bradly, B. C. Mulkerin, A. M. Martin, and H. M. Quiney, “Coupled-pair approach for strongly interacting trapped fermionic atoms,” *Phys. Rev. A* **90**, 023626 (2014).
- [24] Y. Suzuki and K. Varga, *Stochastic Variational Approach to Quantum-Mechanical Few-Body Problems* (Springer, 1998).
- [25] B. Hammond, W. Lester, and P. Reynolds, *Monte Carlo Methods in Ab Initio Quantum Chemistry*, Lecture and Course Notes In Chemistry Series (World Scientific, 1994).
- [26] E. Y. Loh, J. E. Gubernatis, R. T. Scalettar, S. R. White, D. J. Scalapino, and R. L. Sugar, “Sign problem in the numerical simulation of many-electron systems,” *Phys. Rev. B* **41**, 9301 (1990).
- [27] The Supplemental Material at [to be inserted by the editor] contains tables and figures (like Tables I and II, and Figs. 2 and 3) for the $N = 3, 4, 6, 7, 9$, and 10 systems. It also contains figures on the range dependence of the structural properties.
- [28] F. Werner, “Virial theorems for trapped cold atoms,” *Phys. Rev. A* **78**, 025601 (2008).
- [29] R. P. Feynman, “Forces in molecules,” *Phys. Rev.* **56**, 340 (1939).
- [30] S. Tan, “Energetics of a strongly correlated Fermi gas,” *Annals of Physics* **323**, 2952 (2008).
- [31] F. Werner and Y. Castin, “Unitary quantum three-body problem in a harmonic trap,” *Phys. Rev. Lett.* **97**, 150401 (2006).
- [32] J. Carlson, private communication, Feb. and Apr. 2015.
- [33] T. Busch, B.-G. Englert, K. Rzażewski, and M. Wilkens, “Two cold atoms in a harmonic trap,” *Foundations of Physics* **28**, 549 (1998).
- [34] S. T. Rittenhouse, N. P. Mehta, and C. H. Greene,

- “Green’s functions and the adiabatic hyperspherical method,” Phys. Rev. A **82**, 022706 (2010).
- [35] Y. Yan and D. Blume, “Harmonically trapped Fermi gas: Temperature dependence of the Tan contact,” Phys. Rev. A **88**, 023616 (2013).
- [36] D. T. Son, “Three comments on the Fermi gas at unitarity in a harmonic trap,” arXiv:0707.1851.

Supplemental Material

Trapped unitary two-component Fermi gases with up to ten particles

X. Y. Yin¹ and D. Blume¹

¹*Department of Physics and Astronomy, Washington State University, Pullman, Washington 99164-2814, USA*
(Dated: September 15, 2021)

TABLE I. Ground state energy of the (2,1) system at unitarity. Column 2 shows the finite-range energy for the largest basis set considered. The estimated basis set error $\Delta E(r_0)$ is reported in column 3. Columns 4 and 5 report the quantities $E^{(1)}(r_0)$ and $E^{(2)}(r_0)$; errorbars are given in parenthesis. The energy derivatives are calculated for the largest basis set considered. Columns 6-8 report the energies $E_{\text{ZRA},0}(r_0)$, $E_{\text{ZRA},1}(r_0)$, and $E_{\text{ZRA},2}(r_0)$. These energies account for the estimated basis set extrapolation error, i.e., $E(r_0) - \Delta E(r_0)$ is being used to calculate $E_{\text{ZRA},j}(r_0)$ for $j = 0, 1$, and 2. The errorbars of $E_{\text{ZRA},1}(r_0)$ and $E_{\text{ZRA},2}(r_0)$ account for the uncertainties of $E^{(1)}(r_0)$ and $E^{(2)}(r_0)$ but do not account for the uncertainty of $\Delta E(r_0)$. The last row reports the extrapolation of $E_{\text{ZRA},j}(r_0)$ to the zero-range limit.

$\frac{r_0}{a_{\text{ho}}}$	$\frac{E(r_0)}{E_{\text{ho}}}$	$\frac{\Delta E(r_0)}{E_{\text{ho}}}$	$E^{(1)}(r_0) \frac{a_{\text{ho}}}{E_{\text{ho}}}$	$E^{(2)}(r_0) \frac{a_{\text{ho}}^2}{E_{\text{ho}}}$	$\frac{E_{\text{ZRA},0}(r_0)}{E_{\text{ho}}}$	$\frac{E_{\text{ZRA},1}(r_0)}{E_{\text{ho}}}$	$\frac{E_{\text{ZRA},2}(r_0)}{E_{\text{ho}}}$
0.12	4.29594	0.00001	0.1502(2)	-0.91(1)	4.29593	4.27791(2)	4.27137(10)
0.1	4.29276	0.00001	0.1683(5)	-0.87(1)	4.29275	4.27592(5)	4.27155(10)
0.08	4.28923	0.00001	0.1846(9)	-0.68(3)	4.28922	4.27445(7)	4.27227(17)
0.06	4.28538	0.00001	0.199(2)	-0.58(3)	4.28537	4.27341(12)	4.27237(17)
0.04	4.28128	0.00001	0.209(2)	-0.35(3)	4.28127	4.27290(8)	4.27262(10)
0.03	4.27916	0.00001	0.213(5)	-0.23(5)	4.27915	4.27277(15)	4.27266(17)
0.02	4.27702	0.00002	0.214(5)	-0.10(6)	4.27700	4.27271(10)	4.27269(11)
0.01	4.27488	0.00002	0.214(7)	0.09(15)	4.27486	4.27271(7)	4.27272(8)
0					4.27266	4.27271	4.27273

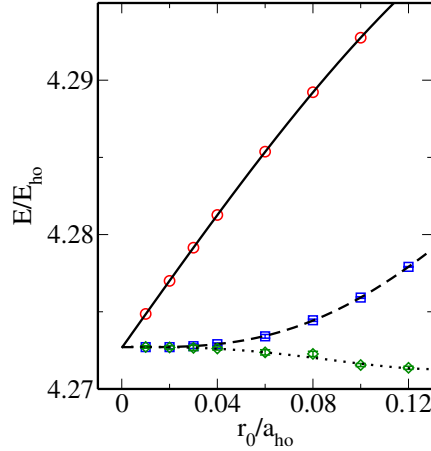


FIG. 1. (Color online) Ground state energy of the (2,1) system at unitarity as a function of r_0 . Circles, squares, and diamonds show the energies $E_{\text{ZRA},0}(r_0)$, $E_{\text{ZRA},1}(r_0)$, and $E_{\text{ZRA},2}(r_0)$, respectively, reported in the last three columns of Table I. The uncertainty of $\Delta E(r_0)$ is not accounted for by the errorbars. Solid, dashed, and dotted lines show polynomial fits to $E_{\text{ZRA},0}(r_0)$, $E_{\text{ZRA},1}(r_0)$, and $E_{\text{ZRA},2}(r_0)$.

TABLE II. Same as Table I but for the (2,2) system at unitarity.

$\frac{r_0}{a_{ho}}$	$\frac{E(r_0)}{E_{ho}}$	$\frac{\Delta E(r_0)}{E_{ho}}$	$E^{(1)}(r_0) \frac{a_{ho}}{E_{ho}}$	$E^{(2)}(r_0) \frac{a_{ho}^2}{E_{ho}}$	$\frac{E_{ZRA,0}(r_0)}{E_{ho}}$	$\frac{E_{ZRA,1}(r_0)}{E_{ho}}$	$\frac{E_{ZRA,2}(r_0)}{E_{ho}}$
0.12	5.21941	0.00005	1.590(16)	-3.26(3)	5.21936	5.02861(192)	5.00515(214)
0.1	5.18697	0.00006	1.654(12)	-3.03(8)	5.18691	5.02149(120)	5.00637(160)
0.08	5.15329	0.00007	1.714(11)	-2.70(14)	5.15322	5.01611(88)	5.00746(133)
0.06	5.11846	0.00010	1.766(16)	-2.22(15)	5.11836	5.01238(96)	5.00838(123)
0.05	5.10068	0.00012	1.789(33)	-1.84(26)	5.10056	5.01113(165)	5.00883(198)
0.04	5.08271	0.00013	1.808(22)	-1.37(32)	5.08258	5.01027(88)	5.00918(114)
0.03	5.06455	0.00016	1.824(31)	-0.96(34)	5.06439	5.00969(93)	5.00926(108)
0.02	5.04623	0.00026	1.834(31)	0.07(48)	5.04597	5.00930(62)	5.00931(72)
0					5.00874	5.00912	5.00939

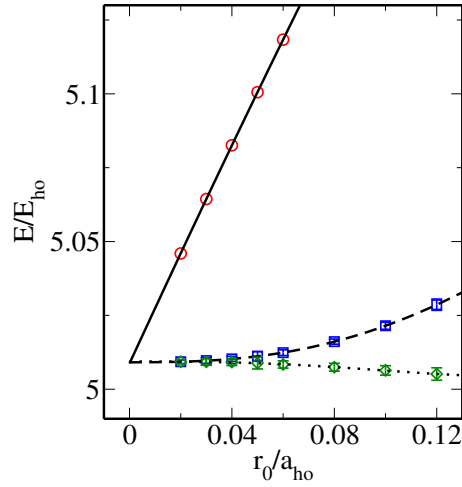


FIG. 2. (Color online) Same as Fig. 1 but for the (2,2) system at unitarity.

TABLE III. Same as Table I but for the (3,3) system at unitarity.

$\frac{r_0}{a_{ho}}$	$\frac{E(r_0)}{E_{ho}}$	$\frac{\Delta E(r_0)}{E_{ho}}$	$E^{(1)}(r_0) \frac{a_{ho}}{E_{ho}}$	$E^{(2)}(r_0) \frac{a_{ho}^2}{E_{ho}}$	$\frac{E_{ZRA,0}(r_0)}{E_{ho}}$	$\frac{E_{ZRA,1}(r_0)}{E_{ho}}$	$\frac{E_{ZRA,2}(r_0)}{E_{ho}}$
0.1	8.6097	0.0009	2.249(8)	-11(1)	8.6088	8.3839(8)	8.3289(58)
0.08	8.5628	0.0012	2.491(14)	-10(1)	8.5616	8.3623(11)	8.3303(43)
0.07	8.5380	0.0018	2.597(16)	-9(1)	8.5362	8.3544(11)	8.3324(36)
0.06	8.5105	0.0021	2.697(21)	-8(2)	8.5084	8.3466(13)	8.3322(49)
0.05	8.4839	0.0023	2.779(35)	-6(2)	8.4816	8.3427(18)	8.3352(43)
0.04	8.4558	0.0028	2.789(62)		8.4530	8.3415(25)	
0.03	8.4281	0.0034	2.791(110)		8.4247	8.3410(33)	
0					8.3413	8.3369	8.3374

TABLE IV. Same as Table I but for the (4,3) system at unitarity.

$\frac{r_0}{a_{ho}}$	$\frac{E(r_0)}{E_{ho}}$	$\frac{\Delta E(r_0)}{E_{ho}}$	$E^{(1)}(r_0) \frac{a_{ho}}{E_{ho}}$	$E^{(2)}(r_0) \frac{a_{ho}^2}{E_{ho}}$	$\frac{E_{ZRA,0}(r_0)}{E_{ho}}$	$\frac{E_{ZRA,1}(r_0)}{E_{ho}}$	$\frac{E_{ZRA,2}(r_0)}{E_{ho}}$
0.1	11.166	0.007	0.94(3)	-11(2)	11.160	11.065(3)	11.010(13)
0.08	11.146	0.009	1.18(12)	-9(2)	11.137	11.043(10)	11.014(16)
0.06	11.120	0.011	1.33(28)		11.108	11.029(17)	
0.04	11.095	0.017	1.13(50)		11.078	11.033(20)	
0					11.004	11.014	

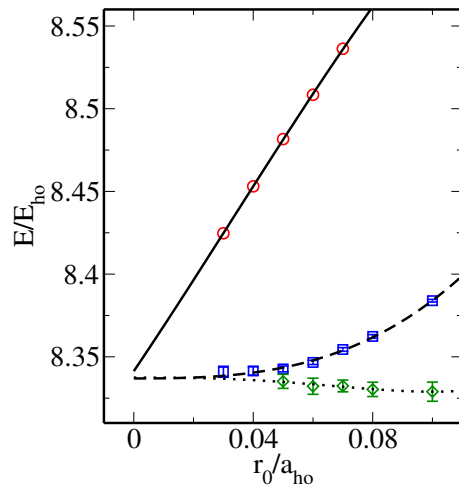


FIG. 3. (Color online) Same as Fig. 1 but for the (3,3) system at unitarity.

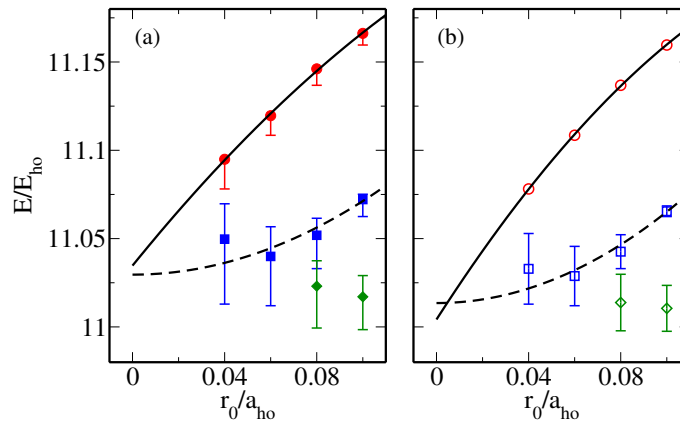


FIG. 4. (Color online) Ground state energy of the (4,3) system at unitarity. (a) Circles, squares, and diamonds show $E_{\text{ZRA},0}(r_0)$, $E_{\text{ZRA},1}(r_0)$, and $E_{\text{ZRA},2}(r_0)$, respectively, for the largest basis set considered. The errorbars of $E_{\text{ZRA},0}(r_0)$ show the estimated basis set error $\Delta E(r_0)$ (see column 3 of Table IV); they extend below the data points but not above. The errorbars of $E_{\text{ZRA},1}(r_0)$ combine the estimated basis set error and the error of $E^{(1)}(r_0)$ (see column 4 of Table IV). Lastly, the errorbars of $E_{\text{ZRA},2}(r_0)$ combine the estimated basis set error, and the errors of $E^{(1)}(r_0)$ and $E^{(2)}(r_0)$ (see column 5 of Table IV). Solid and dashed lines show the extrapolations of $E_{\text{ZRA},0}(r_0)$ and $E_{\text{ZRA},1}(r_0)$ to the zero-range limit. (b) Same quantities as in (a) but corrected for the estimated basis set errors. The open symbols show the energies $E_{\text{ZRA},0}(r_0)$, $E_{\text{ZRA},1}(r_0)$, and $E_{\text{ZRA},2}(r_0)$ reported in the last three columns of Table IV. The uncertainty of $\Delta E(r_0)$ is not accounted for by the errorbars.

TABLE V. Same as Table I but for the (5,4) system at unitarity.

$\frac{r_0}{a_{\text{ho}}}$	$\frac{E(r_0)}{E_{\text{ho}}}$	$\frac{\Delta E(r_0)}{E_{\text{ho}}}$	$E^{(1)}(r_0)$	$\frac{a_{\text{ho}}}{E_{\text{ho}}}$	$E^{(2)}(r_0)$	$\frac{a_{\text{ho}}^2}{E_{\text{ho}}}$	$\frac{E_{\text{ZRA},0}(r_0)}{E_{\text{ho}}}$	$\frac{E_{\text{ZRA},1}(r_0)}{E_{\text{ho}}}$	$\frac{E_{\text{ZRA},2}(r_0)}{E_{\text{ho}}}$
0.12	15.622	0.032	2.09(17)		-16(3)		15.590	15.340(20)	15.224(42)
0.1	15.584	0.045	2.37(18)		-13(4)		15.539	15.302(18)	15.237(38)
0.08	15.536	0.056	2.59(31)				15.480	15.273(25)	
0.06	15.490	0.067	2.14(85)				15.423	15.295(51)	
0							15.227	15.236	

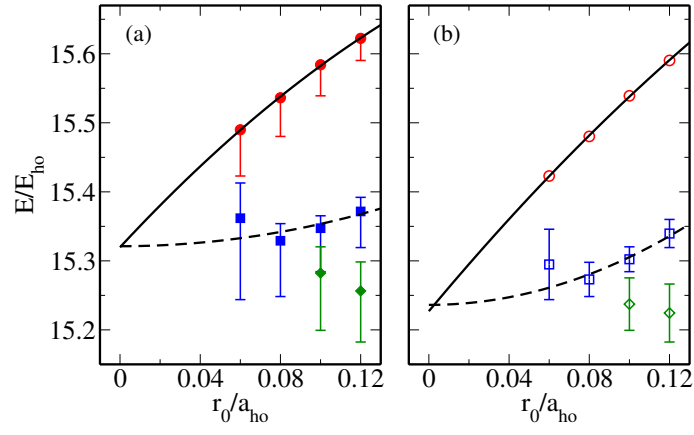


FIG. 5. (Color online) Same as Fig. 4 but for the (5,4) system at unitarity.

TABLE VI. Same as Table I but for the (5,5) system at unitarity.

$\frac{r_0}{a_{ho}}$	$\frac{E(r_0)}{E_{ho}}$	$\frac{\Delta E(r_0)}{E_{ho}}$	$E^{(1)}(r_0)$	$\frac{a_{ho}}{E_{ho}}$	$E^{(2)}(r_0)$	$\frac{a_{ho}^2}{E_{ho}}$	$\frac{E_{ZRA,0}(r_0)}{E_{ho}}$	$\frac{E_{ZRA,1}(r_0)}{E_{ho}}$	$\frac{E_{ZRA,2}(r_0)}{E_{ho}}$
0.12	16.659	0.024	2.64(14)		-28(6)		16.635	16.318(17)	16.127(60)
0.1	16.594	0.030	3.17(25)		-24(4)		16.564	16.247(25)	16.117(45)
0.08	16.522	0.037	3.55(32)				16.485	16.201(26)	
0.06	16.439	0.040	3.40(65)				16.399	16.195(39)	
0							16.095	16.124	

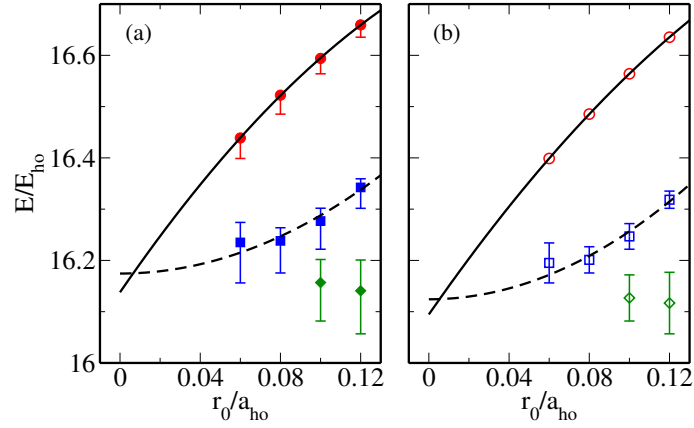


FIG. 6. (Color online) Same as Fig. 4 but for the (5,5) system at unitarity.

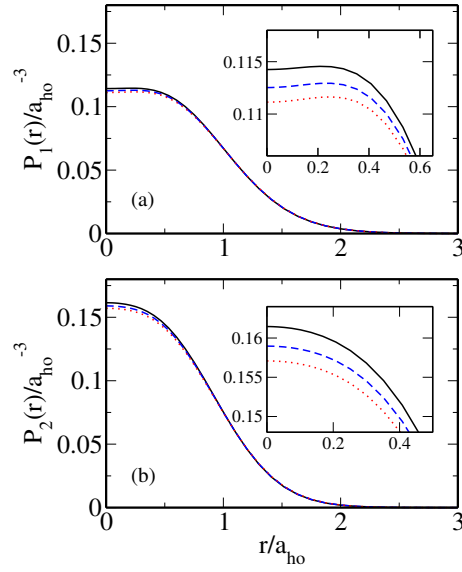


FIG. 7. (Color online) Panels (a) and (b) show the radial densities $P_1(r)$ and $P_2(r)$ of the majority and minority species, respectively, for the ground state of the (3,2) system at unitarity for $r_0 = 0.06a_{\text{ho}}$ (dotted line), $0.04a_{\text{ho}}$ (dashed line), and $0.02a_{\text{ho}}$ (solid line). The insets of panels (a) and (b) show blow-ups of the small r regions.

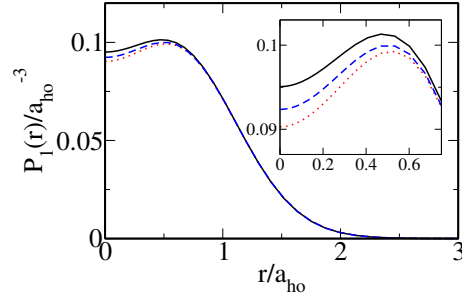


FIG. 8. (Color online) Radial density $P_1(r)$ for the ground state of the (4,4) system at unitarity for $r_0 = 0.1a_{\text{ho}}$ (dotted line), $0.08a_{\text{ho}}$ (dashed line), and $0.06a_{\text{ho}}$ (solid line). The inset shows a blow-up of the small r region.

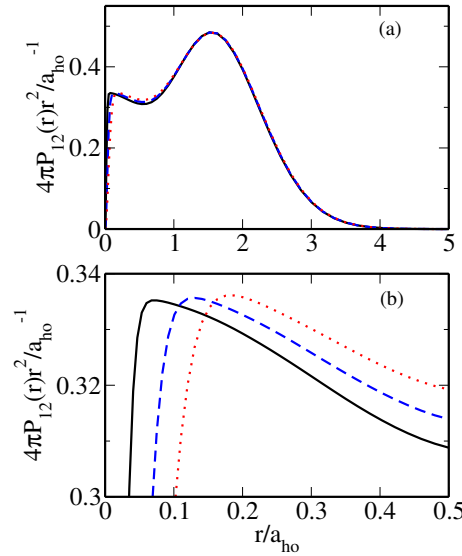


FIG. 9. (Color online) Panel (a) shows the scaled pair distribution function $4\pi P_{12}(r)r^2$ of the ground state for the (3,2) system at unitarity for $r_0 = 0.06a_{\text{ho}}$ (dotted line), $0.04a_{\text{ho}}$ (dashed line), and $0.02a_{\text{ho}}$ (solid line). Panel (b) shows a blow-up of the small r region.

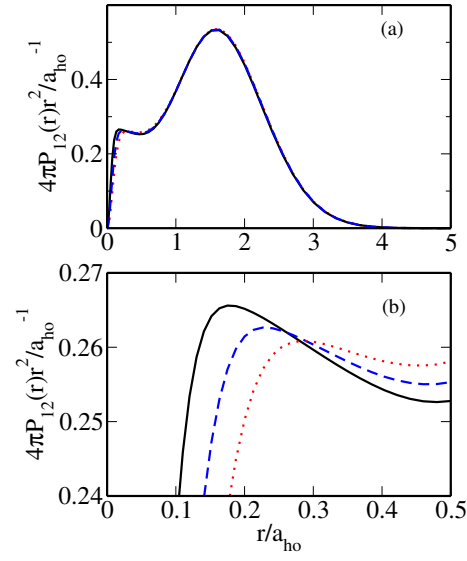


FIG. 10. (Color online) Panel (a) shows the scaled pair distribution function $4\pi P_{12}(r)r^2$ of the ground state for the (4,4) system at unitarity for $r_0 = 0.1a_{\text{ho}}$ (dotted line), $0.08a_{\text{ho}}$ (dashed line), and $0.06a_{\text{ho}}$ (solid line). Panel (b) shows a blow-up of the small r region.